

# Improving the Scaling and Performance of Multiple Time Stepping based Molecular Dynamics with Hybrid Density Functionals

Sagarmoy Mandal<sup>a,b,c</sup>, Ritama Kar<sup>a</sup>, Tobias Klöffel<sup>b,c</sup>, Bernd Meyer<sup>b,c</sup> and Nisanth N. Nair<sup>a,\*</sup>

<sup>a</sup>Department of Chemistry, Indian Institute of Technology Kanpur (IITK), 208016 Kanpur, India

<sup>b</sup>Interdisciplinary Center for Molecular Materials and Computer Chemistry Center, Friedrich-Alexander-Universität Erlangen-Nürnberg (FAU), Ngölsbachstr. 25, 91052 Erlangen, Germany

<sup>c</sup>Erlangen National High Performance Computing Center (NHR@FAU), Friedrich-Alexander-Universität Erlangen-Nürnberg, Martensstr. 1, 91058 Erlangen, Germany

## ARTICLE INFO

### Keywords:

*Ab initio* molecular dynamics

Hybrid functionals

CPMD

Task Group

## ABSTRACT

Density functionals at the level of the Generalized Gradient Approximation (GGA) and a plane-wave basis set are widely used today to perform *ab initio* molecular dynamics (AIMD) simulations. Going up in the ladder of accuracy of density functionals from GGA (2<sup>nd</sup> rung) to hybrid density functionals (4<sup>th</sup> rung) is much desired pertaining to the accuracy of the latter in describing structure, dynamics, and energetics of molecular and condensed matter systems. On the other hand, hybrid density functional based AIMD simulations are about two orders of magnitude slower than GGA based AIMD for systems containing  $\sim 100$  atoms using  $\sim 100$  compute cores. Two methods, namely MTACE and *s*-MTACE, based on a multiple time step integrator and adaptively compressed exchange operator formalism are able to provide a speed-up of about 7–9 in performing hybrid density functional based AIMD. In this work, we report an implementation of these methods using a task-group based parallelization within the CPMD program package, with the intention to take advantage of the large number of compute cores available on modern high-performance computing platforms. We present here the boost in performance achieved through this algorithm. This work also identifies the computational bottleneck in the *s*-MTACE method, and proposes a way to overcome that.

## 1. Introduction

Kohn-Sham density functional theory (KS-DFT) and plane wave (PW) based *ab initio* molecular dynamics (AIMD) techniques are widely used in investigating structural and dynamical properties of condensed matter systems.[1, 2, 3, 4, 5] The accuracy of the KS-DFT calculations crucially depends on the choice of exchange-correlation (XC) functionals. Owing to improved accuracy, hybrid functionals are preferred over the commonly used XC functionals using the Generalized Gradient Approximation (GGA).[6, 7, 8] Hybrid functionals incorporate a certain fraction of the Hartree-Fock (HF) exchange to the GGA exchange.[8, 9, 10, 11, 12] They give better prediction of energies, structures, electronic properties, reaction barriers, band gap of solids and dynamical properties of liquids.[10, 11, 13, 12, 14, 15, 16, 17, 18, 19, 20, 21, 22, 23, 24, 25, 26, 27, 28, 29, 30, 31] However, the prohibitively high computational cost associated with HF exchange energy evaluation makes the hybrid functionals and PW based AIMD simulations extremely time consuming.[32] This limits the routine use of hybrid functionals and PW based AIMD simulations for large condensed matter systems.

A number of promising strategies have been proposed so far to speed-up such calculations, which can be broadly divided into two categories. The first set of techniques in-

troduce some approximations in the evaluation of the HF exchange energy, thereby reducing the computational cost. Several works have been reported in this direction using localized orbitals,[33, 25, 26, 27, 34, 35, 36, 37, 38, 16, 39, 31, 40, 41] multiple time step (MTS) algorithms,[42, 43, 44, 45, 29, 30] coordinate scaling,[46, 47] and other strategies.[48, 49, 50, 51] The other group of methods improve the performance by employing massively parallel algorithms.[52, 53, 54, 55] A combination of both the strategies has been also used to achieve remarkable speed-up.[40, 41]

Recently, we proposed an efficient and robust method[45, 29] for performing hybrid functionals and PW based AIMD. We employed a MTS integrator[2] scheme based on the adaptively compressed exchange (ACE) [56, 57] operator formalism. To take advantage of the ACE operator formalism, we partitioned the ionic forces into computationally cheap fast forces using an approximated ACE operator and computationally costly slow forces due to corrections to the approximated ACE operator. We denote this method as MTACE hereafter. This approach provided a significant speed-up in AIMD simulations by decreasing the number of exact exchange evaluations. Subsequently, we improved the efficiency of this method[30] by employing localized orbitals. In particular, we used the selected column of the density matrix (SCDM)[58] method to obtain localized orbitals, and we used these localized orbitals to build the ACE operator.[59] We will be denoting this method as *s*-MTACE. These methods could speed-up the calculations up to an order of magnitude without compromising on accuracy.[30, 29, 45] Both MTACE and

\*Corresponding author

✉ mandal.sagarmoy@fau.de (S. Mandal); kritama@iitk.ac.in (R. Kar); tobias.kloeffel@fau.de (T. Klöffel); bernd.meyer@fau.de (B. Meyer); nnair@iitk.ac.in (N.N. Nair)

ORCID(s): 0000-0002-3481-8009 (B. Meyer); 0000-0001-8650-8873 (N.N. Nair)

s-MTACE methods are found to reproduce the structure and dynamics of bulk water and free energetics of chemical reactions in solutions correctly.

In the PW based KS-DFT codes, wavefunctions and KS potentials can be in real and/or reciprocal space, and these representations are inter-converted with the help of three dimensional (3D) FFTs. For the optimal performance of the 3D parallel FFTs, PW implementations use a slab decomposition of the real 3D FFT grids to distribute the data. For instance, the 3D FFT grids are distributed along the  $X$ -direction and the  $YZ$  planes are distributed among the MPI tasks (or compute-cores). Weak scaling performance of such implementations is limited by the number of grid points along the  $X$  direction. For typical DFT calculations today, the number of grid points along any direction is few hundreds, while the number of available compute cores on any modern day supercomputing resource is of the order of few thousands to millions. Thus, slab decomposition based FFTs cannot take the full advantage of the large computational resources available today. To overcome this, a task group based parallelization strategy was proposed.[52, 60] This strategy implemented in the CPMD[61] program is called CP Group. In the CP Group implementation of HF exchange computation, the available processors are divided into several task groups and the array that holds the wavefunctions is replicated among these groups. The total workload of the HF exchange energy computation is divided into several parts and they are distributed evenly among these task groups. Finally, a global summation across these groups provides the total contribution to the HF exchange energy.

In the present work, we report the implementations of the MTACE and s-MTACE methods together with CP Group within the CPMD program and we present their performance. In particular, we present the scaling behaviour of the MTACE and s-MTACE methods on a large number of CPU compute cores. We will be demonstrating here that a significant improvement in the performance of these methods can be achieved through such an approach.

## 2. Methods

### 2.1. HF Exchange Operator

In conventional KS-DFT calculations using hybrid density functionals and plane waves, evaluation of the HF exchange contributes the most to the total computational time. The HF exchange operator  $\mathbf{V}_X$  is defined as

$$\mathbf{V}_X = - \sum_j^{N_{\text{orb}}} \frac{|\psi_j\rangle\langle\psi_j|}{r_{12}}, \quad (1)$$

where,  $\{|\psi_j\rangle\}$  is the set of occupied KS orbitals.  $N_{\text{orb}}$  is the total number of occupied orbitals and  $r_{12} = |\mathbf{r}_1 - \mathbf{r}_2|$ . The

$\mathbf{V}_X$  operator is applied on a KS orbital  $|\psi_i\rangle$  as

$$\begin{aligned} \mathbf{V}_X|\psi_i\rangle &= - \sum_j^{N_{\text{orb}}} |\psi_j\rangle \langle\psi_j|(r_{12})^{-1}|\psi_i\rangle \\ &= - \sum_j^{N_{\text{orb}}} v_{ij}(\mathbf{r}_1)|\psi_j\rangle, \quad i = 1, \dots, N_{\text{orb}} \end{aligned} \quad (2)$$

with

$$v_{ij}(\mathbf{r}_1) = \langle\psi_j|(r_{12})^{-1}|\psi_i\rangle. \quad (3)$$

The HF exchange energy is calculated as

$$E_X^{\text{HF}} = - \sum_{i,j}^{N_{\text{orb}}} \langle\psi_i|v_{ij}(\mathbf{r}_1)|\psi_j\rangle. \quad (4)$$

For an optimal performance,  $v_{ij}(\mathbf{r})$  is usually evaluated in reciprocal space.[32, 33] The computational cost for doing Fourier transform scales as  $N_{\text{PW}} \log N_{\text{PW}}$  using the Fast Fourier Transform (FFT) technique, where  $N_{\text{PW}}$  is total number of PWs. Therefore, the total computational cost for the evaluation of exchange energy scales as  $N_{\text{orb}}^2 N_{\text{PW}} \log N_{\text{PW}}$ ,[32] as  $v_{ij}(\mathbf{r})$  has to be evaluated  $N_{\text{orb}}^2$  times. This scaling is the reason behind the computational time required for hybrid functional calculations.

### 2.2. ACE Operator

Lin Lin [56, 57] introduced a low rank decomposition of the  $\mathbf{V}_X$  operator in the form

$$\mathbf{V}_X^{\text{ACE}} = - \sum_k^{N_{\text{orb}}} |P_k\rangle\langle P_k|.$$

Here, the set of ACE projection vectors  $\{|P_k\rangle\}$  can be computed by a decomposition of the  $\mathbf{V}_X$  operator, see Ref.[56, 45] for details. The construction of  $\{|P_k\rangle\}$  requires evaluation of  $\{\mathbf{V}_X|\psi_i\rangle\}$ , which follows the same computationally demanding procedure requiring  $N_{\text{orb}}^2$  evaluations of  $v_{ij}(\mathbf{r})$  as discussed in the previous section.[56] However, once the  $\mathbf{V}_X^{\text{ACE}}$  operator is constructed, it can be easily applied on KS orbitals through the evaluation of  $N_{\text{orb}}^2$  inner products as

$$\mathbf{V}_X^{\text{ACE}}|\psi_i\rangle = - \sum_k^{N_{\text{orb}}} |P_k\rangle \langle P_k|\psi_i\rangle, \quad i = 1, \dots, N_{\text{orb}}. \quad (5)$$

The advantage of the ACE approach lies in the fact that the application of the  $\mathbf{V}_X^{\text{ACE}}$  operator on each KS orbitals consumes much less time as compared to the  $\mathbf{V}_X$  operator. Such a low rank decomposition can be used in multiple ways to speed-up the HF exchange energy calculations.

### 2.3. MTACE Method

The MTACE method introduced by some of the authors of this paper [45, 29] uses the ACE formalism in the framework of the MTS scheme for speeding-up hybrid functional based AIMD. The self consistent field (SCF) procedure is

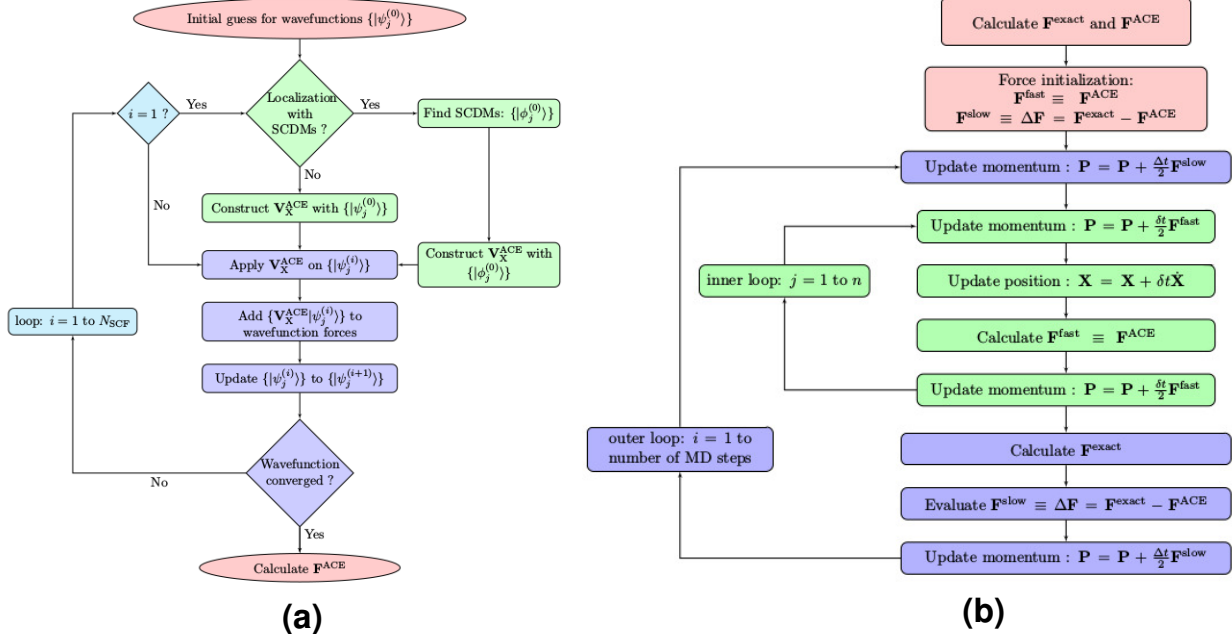


**Figure 1:** Flowcharts of the MTACE and s-MTACE algorithms: (a) SCF procedure in the s-MTACE method, construction of  $\mathbf{V}_X^{\text{ACE}}$  in the first SCF step is done using SCDM-localized orbitals. (b) MTS integration used to perform AIMD simulations.

modified to take the benefits of the ACE operator. In the first SCF step, the ACE operator is constructed after the decomposition of  $\mathbf{V}_X$ , which is a computationally demanding step as it involves the computation of  $\mathbf{V}_X$ . However, for the remaining SCF steps, we use the same ACE operator constructed at the first SCF step without recalculating it. After reaching complete SCF convergence, we compute the ionic forces  $\mathbf{F}^{\text{ACE}}$ . It is to be noted that the optimized wavefunction is most certainly different to the wavefunction which one would obtain if the ACE operator is updated every SCF step. As a result,  $\mathbf{F}^{\text{ACE}} \neq \mathbf{F}^{\text{exact}}$ , where  $\mathbf{F}^{\text{exact}}$  is the ionic force computed using the HF  $\mathbf{V}_X$  operator. We take care of this difference in forces within the MTS algorithm as explained later. The flowchart for this modified SCF procedure is shown in Figure 1(a).

In the MTACE scheme, ionic force component can be written as

$$F_K^{\text{exact}} = F_K^{\text{ACE}} + \Delta F_K, \quad K = 1, \dots, 3N_{\text{atom}} \quad (6)$$

with  $\Delta F_K = F_K^{\text{exact}} - F_K^{\text{ACE}}$ . In our earlier works,[45, 29] we have shown that differences in the ionic force components of  $\mathbf{F}^{\text{exact}}$  and  $\mathbf{F}^{\text{ACE}}$  are very small and it is justified to consider  $\mathbf{F}^{\text{ACE}}$  as fast and  $\Delta \mathbf{F}$  as slow:

$$\begin{aligned} F_K^{\text{slow}} &\equiv \Delta F_K = F_K^{\text{exact}} - F_K^{\text{ACE}}, \quad \text{and} \\ F_K^{\text{fast}} &\equiv F_K^{\text{ACE}}. \end{aligned} \quad (7)$$

Finally, we employ the reversible reference system propagator algorithm (r-RESPA) scheme[62] which allows us to compute the computationally costly  $\Delta \mathbf{F}$  less frequently, in fact every  $n$  MD steps, as compared to computationally cheaper  $\mathbf{F}^{\text{ACE}}$ , resulting in speeding-up the calculations as

shown in Figure 1(b). For more details, see Ref. [45]. We could achieve a speed-up of about 7 times using this method for a periodic system containing  $\sim 100$  atoms employing only 120 compute cores.

## 2.4. s-MTACE Method

A modification of the MTACE method, namely s-MTACE, was subsequently proposed,[30] wherein localized SCDM orbitals[58] are used for the construction of the  $\mathbf{V}_X^{\text{ACE}}$  operator, see Figure 1a. Based on a rank-revealing QR factorization of  $\Psi^*$ , where  $\Psi$  is the matrix with all the occupied KS orbitals, the SCDM method constructs linearly independent columns of the density matrix  $\Gamma = \Psi\Psi^*$  without computing the full  $\Gamma$  matrix. The selected columns of  $\Gamma$  are then used to construct the set of orthonormal localized SCDMs  $\{\phi_i\}$ . By screening  $\{\phi_i\}$  based on their spatial overlap, it is possible to achieve a substantial reduction in the number of orbitals involved in the evaluation of  $\{\mathbf{V}_X|\psi_i\rangle\}$  in Equation (2). We screen the orbitals using the criteria

$$\int d\mathbf{r} |\phi_i(\mathbf{r})\phi_j^*(\mathbf{r})| \geq \rho_{\text{cut}}.$$

We have reported that this procedure substantially reduces the cost of  $\mathbf{V}_X^{\text{ACE}}$  operator construction.[30] It has been shown that s-MTACE can achieve one order of magnitude speed-up for a system containing  $\sim 100$  atoms using 120 compute cores.

## 2.5. s'-MTACE Method

The rank-revealing QR factorization required for the construction of SCDMs is the most time consuming step of the SCDM procedure. To speed-up these calculations, we

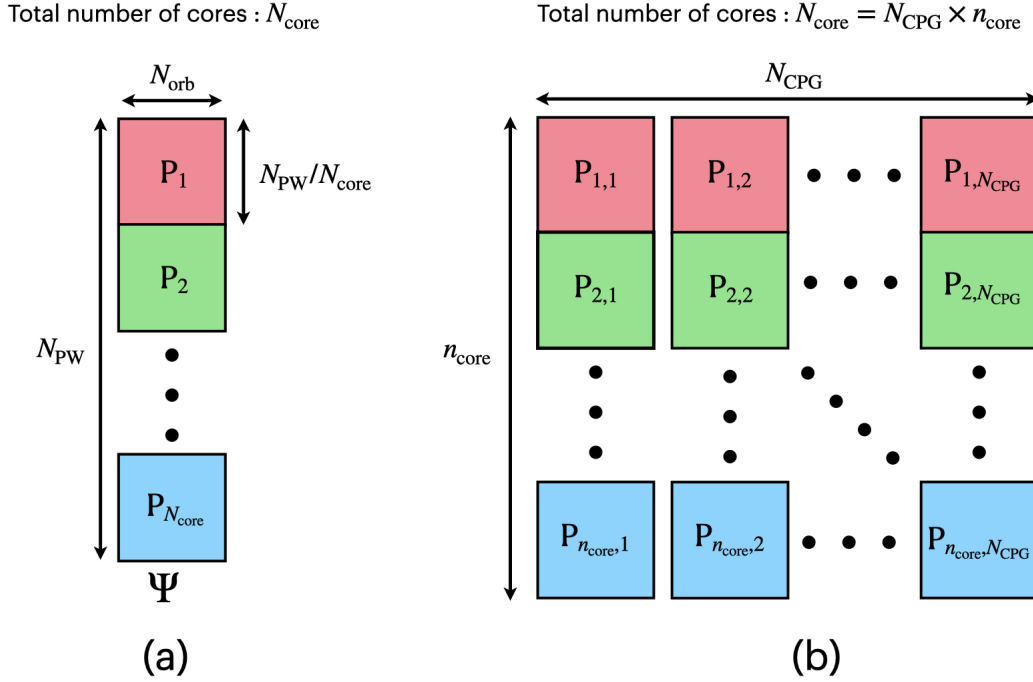


**Figure 2:** (a) Conventional distribution of the  $\Psi$  matrix with  $N_{\text{core}}$  compute-cores. The total number of rows ( $N_{\text{PW}}$ ) is distributed among these available compute-cores. The part of the matrix residing in different compute-core is shown with different color. (b) The CP Group data distribution is shown for  $N_{\text{core}}$  compute-cores. Total number of compute-cores are divided into  $N_{\text{CPG}}$  groups. Each group contains  $n_{\text{core}}$  compute-cores to distribute the  $\Psi$  matrix. Each compute-core contains  $N_{\text{PW}}/n_{\text{core}}$  rows of the  $\Psi$  matrix.

employ parallel ScaLAPACK routines. However, these procedures scale poorly when using a large number of processors.

Giannozzi and co-workers[59] proposed a way to improve the computational efficiency of finding localized SCDMs. In this method, one pre-selects a column of the density matrix based on the electron density and the gradient of the electron density. A column with index  $i$  is selected only if

$$\rho(\mathbf{r}_i) > \langle \rho \rangle \quad \text{and} \quad \nabla \rho(\mathbf{r}_i) < \langle \nabla \rho \rangle .$$

Here,  $\langle \rho \rangle$  and  $\langle \nabla \rho \rangle$  are the average electron density and average gradient of the electron density over the grid points. This pre-screening scheme substantially reduces the number of grid points which are to be considered for QR factorization. Now, the call to the ScaLAPACK routine involves a smaller size matrix  $\Psi^*$ , thereby improving the performance. A successful implementation of this procedure is already available in the Quantum ESPRESSO code.[63, 64] We have implemented the same approach in the CPMD program to improve the performance of the s-MTACE method. This will be referred as  $s'$ -MTACE method hereafter.

## 2.6. CP Groups Approach

Let us consider that each of the  $N_{\text{orb}}$  KS orbitals possesses  $N_{\text{PW}}$  PW coefficients and  $N_{\text{core}}$  compute-cores are available, then each compute core stores  $N_{\text{PW}}/N_{\text{core}}$  rows of the wavefunction matrix  $\Psi$  in a typical implementation of the slab decomposition, see Figure 2(a). In the CP Group

approach, as shown in Figure 2(b), the total number of available compute cores  $N_{\text{core}}$  divided into  $N_{\text{CPG}}$  groups. Each of such a CP Group possesses  $n_{\text{core}} = N_{\text{core}}/N_{\text{CPG}}$  compute cores. A copy of the whole  $\Psi$  matrix is kept with every group, distributed among the  $n_{\text{core}}$  compute cores within that group. As a result, each compute core of a group keeps  $N_{\text{PW}}/n_{\text{core}}$  rows of the  $\Psi$  matrix. The workload across the task groups is parallelized over the orbital pairs entering the exchange integral in such a manner that computations within each CP Group is restricted to a subset of orbital pairs. Through this, computation of  $v_{ij}(\mathbf{r})$  (in Equation 3), which has to be performed for all the orbital pairs, can now be done in chunks across the CP Group. Finally, a global sum across the groups is performed to evaluate the full exchange operator. The replication of the whole  $\Psi$  matrix among the CP Groups minimizes the inter group communication. It has been shown that the CP Group approach can be made use to achieve excellent scaling performance in hybrid functional based calculations on several thousands of compute cores.[52, 60]

## 3. Results and Discussion

We are presenting here the results of scaling tests of the MTACE, s-MTACE and  $s'$ -MTACE methods using the CP Groups implementation. Benchmark calculations were carried out for periodic supercells with 32, 64, and 128 water molecules (Table 1).

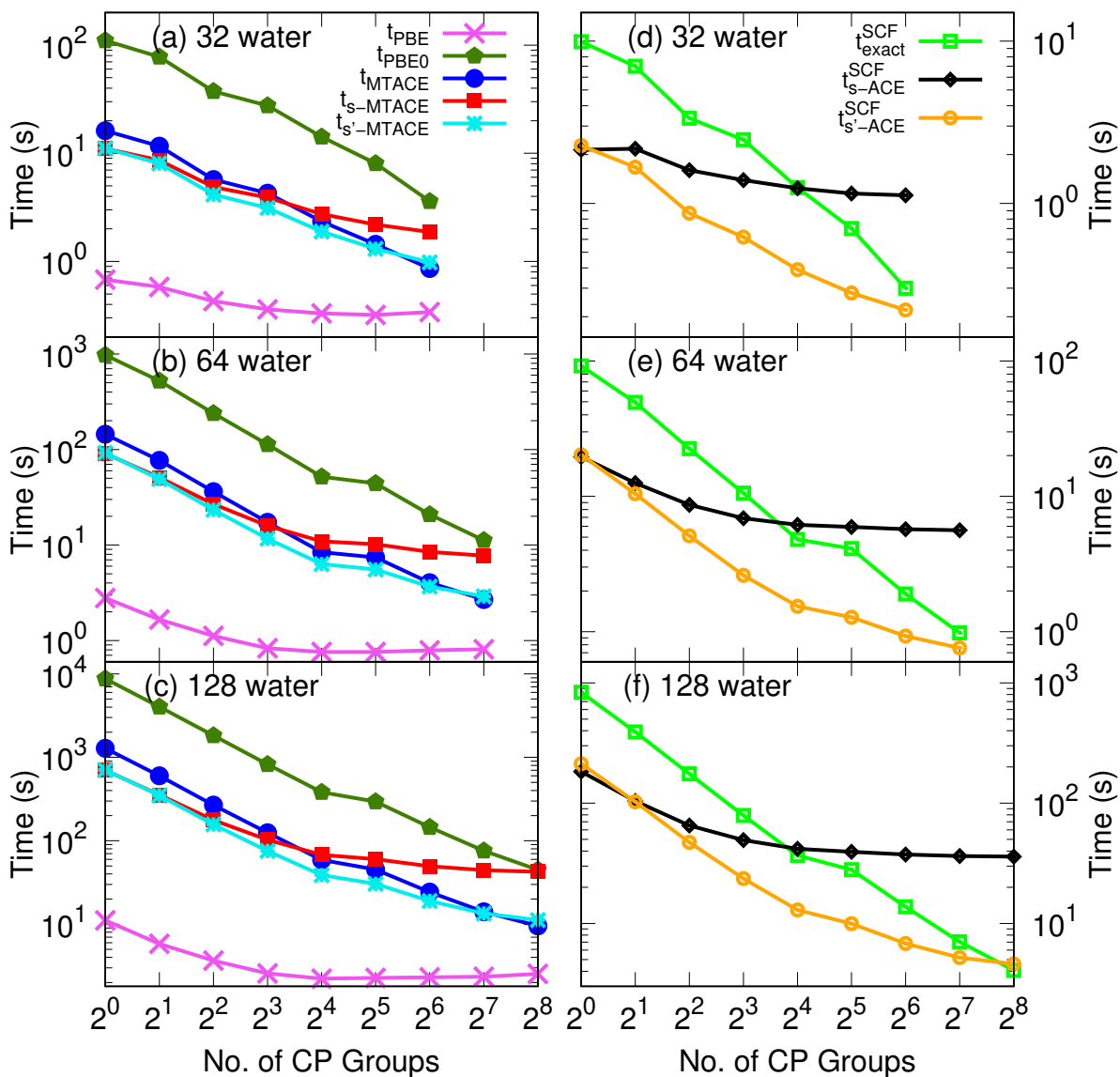


**Figure 3:** Scaling of the average computational time per BOMD step and average computational time per SCF step for periodic systems containing 32, 64 and 128 water molecules.  $t_{\text{PBE}}$ ,  $t_{\text{PBE0}}$ ,  $t_{\text{MTACE}}$ ,  $t_{\text{s-MTACE}}$  and  $t_{\text{s'-MTACE}}$  are the average computing time per MD step in **PBE**, **PBE0**, **MTACE**, **s-MTACE** and **s'-MTACE** runs.  $t_{\text{exact}}^{\text{SCF}}$  is the average computing time per SCF step during the computation of  $\mathbf{F}^{\text{exact}}$ .  $t_{\text{s-ACE}}^{\text{SCF}}$  and  $t_{\text{s'-ACE}}^{\text{SCF}}$  are the average computing time for the first SCF step during the computation of  $\mathbf{F}^{\text{s-ACE}}$  and  $\mathbf{F}^{\text{s'-ACE}}$ . The number of compute cores per CP Group ( $n_{\text{core}}$ ) are 120, 144 and 192 for systems containing 32, 64 and 128 water molecules, respectively.

All the methods and algorithms presented earlier were implemented in a modified version of the CPMD 4.3 program,[61, 65] and adapted for the existing CP Group implementation within the program. We used PBE0 [13] (hybrid) and PBE [66] (GGA) functionals for all the computations. Core electrons were accounted by using norm-conserving Troullier Martin pseudopotentials. [67] A cutoff energy of 80 Ry was used to expand the wavefunctions in the PW basis set. We carried out Born-Oppenheimer molecular dynamics (BOMD) simulations and the wavefunction convergence criteria in SCF calculations was set to  $10^{-6}$  au for

the wavefunction gradients. At every MD step, initial guess of the wavefunctions was constructed based on the Always Stable Predictor Corrector extrapolation scheme[68] with order 5. For standard PBE and PBE0 calculations, the standard Velocity Verlet scheme was employed with a timestep of  $\Delta t = 0.48$  fs. However, for the PBE0 runs with the MTS scheme,  $\delta t = 0.48$  fs and  $\Delta t = 7.2$  fs (i.e.,  $n = 15$ ) were taken as the smaller and larger time steps, respectively. We use the labels **PBE**, **PBE0**, **MTACE**, **s-MTACE**, and **s'-MTACE** to indicate different methods used in this work, see Table 2.

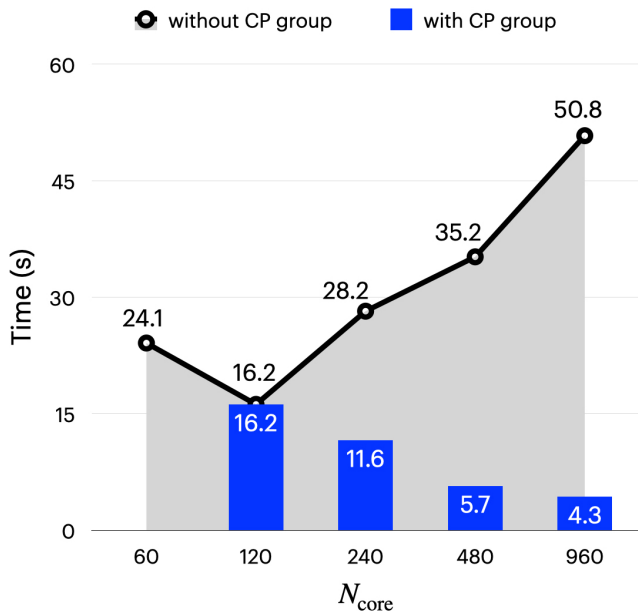


**Figure 4:** CPU time per MD step for **MTACE** with increasing number of compute cores ( $N_{\text{core}}$ ) for a periodic 32-water model. Black line shows the scalability of the method without CP Group, and the blue bars display the scaling when CP Group was used. One MD step is 0.48 fs.

**Table 1**

Details of the liquid water systems used in our benchmarking studies.  $N_{\text{water}}$  is the number of water molecules,  $N_{\text{atom}}$  is the number of atoms,  $N_{\text{orb}}$  is the number of orbitals,  $N_{\text{grid}}$  is the number of grid points,  $N_{\text{PW}}^{\text{wave}}$  is the number of PWs for wavefunction cutoff, and  $N_{\text{PW}}^{\text{density}}$  is the number of PWs for density cutoff.

$N_{\text{water}}$	$N_{\text{atom}}$	$N_{\text{orb}}$	$N_{\text{grid}}$	Cell size (Å)	$N_{\text{PW}}^{\text{wave}}$	$N_{\text{PW}}^{\text{density}}$
32	96	128	120	9.85	39103	311563
64	192	256	144	12.41	77978	623469
128	384	512	192	15.64	156181	1247311

**Table 2**

Different simulation runs; Note: for the case of MTS based BOMD, we have  $n > 1$ , where  $n = \Delta t / \delta t$ .

Simulation Label	Functional	$n$	BOMD Scheme
<b>PBE</b>	GGA/PBE	1	Conventional
<b>PBE0</b>	Hybrid/PBE0	1	Conventional
<b>MTACE</b>	Hybrid/PBE0	15	MTACE
<b>s-MTACE</b>	Hybrid/PBE0	15	s-MTACE
<b>s'-MTACE</b>	Hybrid/PBE0	15	s'-MTACE

All the benchmark calculations presented here were performed on SuperMUC-NG located at Leibniz Supercomputing Center (LRZ). The compute nodes are equipped with two Intel® Skylake Xeon Platinum 8174 processors (24 compute cores per processor). Each compute node has 48 compute cores and 96 GB memory. The nodes are interconnected through a fast Intel® OmniPath network with 100 Gbit/s

**Table 3**

The number of BOMD steps over which the average compute-times were calculated.  $N_{\text{MD}}^X$  is the total number of MD steps with method X.  $\rho_{\text{cut}}$  is the cutoff used for the screening of the SCDMs in **s-MTACE** and **s'-MTACE** runs.  $n_{\text{core}}$  is the number of compute cores per task group.

$N_{\text{water}}$	$N_{\text{MD}}^{\text{PBE}}$	$N_{\text{MD}}^{\text{PBE0}}$	$N_{\text{MD}}^{\text{MTACE}}$	$N_{\text{MD}}^{\text{s-MTACE}}$	$N_{\text{MD}}^{\text{s'-MTACE}}$	$\rho_{\text{cut}}$	$n_{\text{core}}$
32	500	300	300	300	300	$2.5 \times 10^{-2}$	120
64	300	50	150	150	150	$1.0 \times 10^{-2}$	144
128	300	20	75	75	75	$2.0 \times 10^{-3}$	192

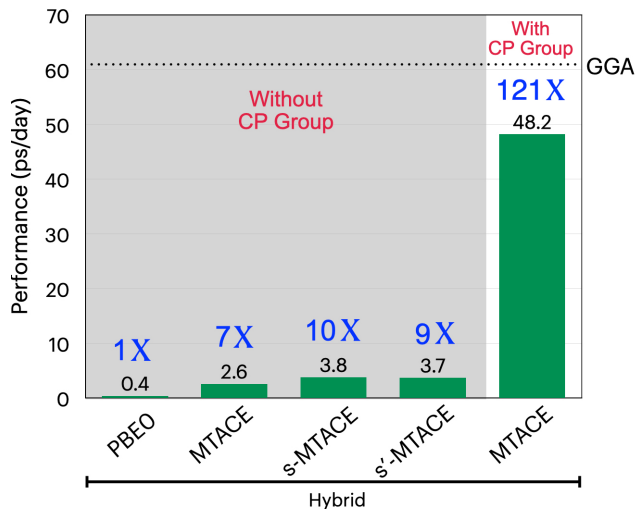


**Figure 5:** Best performance of the methods discussed in this article for the 32 water system. Performance has been measured as the length of the trajectory (in ps) generated in one day. A time step of 0.48 fs was only used as H atom mass was taken as 1 amu. Grey area highlights the schemes where CP Group was not used. 120 compute cores were used for all the calculations. Dotted black line indicates the performance of the GGA calculations with 120 compute cores. The best performance with CP Group was obtained for the **MTACE** on 7680 compute cores. Effective speed-up compared to PBE0 is also indicated here (blue).

speed.

In Table 3, we give the number of steps for which average compute timings were calculated and the values of  $\rho_{\text{cut}}$  for the s-MTACE runs. For an ideal load balancing, the number of compute cores per CP Group ( $n_{\text{core}}$ ) is chosen to be equal to the number of grid points in the X-direction. We chose  $n_{\text{core}}$  as 120, 144 and 192 for systems containing 32, 64 and 128 water molecules, respectively, see Table 3.

The average computational time per BOMD step is reported in Table 4 for the **PBE**, **PBE0**, **MTACE** and **s-MTACE** methods. Also, the scaling is shown in Figure 3. First, we observe that the **PBE** calculations have poor scaling with CP Groups for all the systems. This is expected as these calculations lack enough computationally scalable work that can be distributed over the CP Groups. In fact due to the extra overhead of communication and synchroni-

**Table 4**

Average computational time per BOMD step and average computational time per SCF step for periodic systems containing 32, 64 and 128 water molecules.  $N_{\text{water}}$  is the number of water molecules,  $N_{\text{core}}$  is the total number of CPU compute cores,  $N_{\text{node}}$  is the total number of compute nodes,  $N_{\text{CPG}}$  is the number of TASK groups.  $t_{\text{PBE}}$  is the average computing time per MD step using GGA (PBE) functional.  $t_{\text{PBE0}}$ ,  $t_{\text{MTACE}}$ ,  $t_{\text{s-MTACE}}$  and  $t_{\text{s'-MTACE}}$  are the average computing time per MD step using **PBE0**, **MTACE**, **s-MTACE** and **s'-MTACE** methods.  $t_{\text{exact}}^{\text{SCF}}$  is the average computing time per SCF step during the computation of  $\mathbf{F}^{\text{exact}}$ .  $t_{\text{s-ACE}}^{\text{SCF}}$  and  $t_{\text{s'-ACE}}^{\text{SCF}}$  are the average computing time for the first SCF step during the computation of  $\mathbf{F}^{\text{s-ACE}}$  and  $\mathbf{F}^{\text{s'-ACE}}$ . All the times reported are in seconds. Calculations were done with 48 compute cores per node, except for the case with  $N_{\text{water}} = 32$  and  $N_{\text{CPG}} = 1$  case where 24 compute cores per node were used.

$N_{\text{water}}$	$N_{\text{core}}$	$N_{\text{node}}$	$N_{\text{CPG}}$	$t_{\text{PBE}}$	$t_{\text{PBE0}}$	$t_{\text{MTACE}}$	$t_{\text{s-MTACE}}$	$t_{\text{s'-MTACE}}$	$t_{\text{exact}}^{\text{SCF}}$	$t_{\text{s-ACE}}^{\text{SCF}}$	$t_{\text{s'-ACE}}^{\text{SCF}}$
32	120	5	1	0.68	110.19	16.20	11.05	11.12	9.92	2.14	2.27
	240	5	2	0.58	77.88	11.62	8.61	8.06	7.00	2.17	1.67
	480	10	4	0.43	37.38	5.71	4.88	4.15	3.35	1.60	0.87
	960	20	8	0.36	27.64	4.27	3.90	3.12	2.47	1.39	0.62
	1920	40	16	0.33	14.19	2.34	2.74	1.89	1.25	1.24	0.39
	3840	80	32	0.32	8.04	1.44	2.19	1.31	0.70	1.15	0.28
	7680	160	64	0.34	3.60	0.86	1.87	0.98	0.30	1.12	0.22
64	144	3	1	2.79	974.08	144.42	90.77	92.14	91.98	19.61	20.27
	288	6	2	1.66	523.59	76.90	50.97	48.85	49.42	12.52	10.46
	576	12	4	1.12	239.36	36.25	26.86	23.38	22.52	8.66	5.11
	1152	24	8	0.83	113.13	17.28	15.93	11.66	10.55	6.90	2.61
	2304	48	16	0.76	51.79	8.40	10.92	6.31	4.81	6.16	1.54
	4608	96	32	0.76	44.14	7.40	10.20	5.55	4.11	5.95	1.28
	9216	192	64	0.79	20.91	4.04	8.46	3.67	1.90	5.72	0.93
18432	384	128	0.81	11.19	2.69	7.73	2.90	0.98	5.62	0.76	
128	192	4	1	11.12	8776.64	1285.86	699.56	708.00	837.51	183.01	212.59
	384	8	2	5.83	4039.04	600.21	355.45	348.78	391.59	104.11	102.83
	768	16	4	3.66	1829.83	268.16	176.99	157.06	175.60	65.23	47.26
	1536	32	8	2.57	823.68	124.82	102.89	75.66	78.96	49.24	23.61
	3072	64	16	2.22	383.01	58.84	67.84	38.82	36.80	41.70	12.94
	6144	128	32	2.27	294.42	45.25	60.08	30.44	27.96	39.44	9.95
	12288	256	64	2.31	145.67	24.25	49.56	19.02	13.73	37.41	6.81
24576	512	128	2.35	75.79	14.11	44.41	13.43	7.03	36.32	5.20	
49152	1024	256	2.54	44.80	9.55	42.37	11.22	4.08	35.92	4.61	

sation, we notice small increase in computational time per MD step with large number of CP Groups. However, for all the other three methods which use hybrid functionals, we notice considerable improvements in the performance with increase in CP Groups. Noticeably, **PBE0** scales almost perfectly with the number of CP Groups. The scaling behavior of **MTACE** is also as good as **PBE0**. It is clear that the scaling of **MTACE** without the CP Group approach is poor when more than 120 compute cores are used for the 32 water system (Figure 4).

From Table 4, we observe that the ratio of the average computing time per MD step for **MTACE** and **PBE** ( $t_{\text{MTACE}}/t_{\text{GGA}}$ ) decreases with increasing number of CP Group. This is a consequence of the fact that the **MTACE** calculations are scaling well with CP Groups as compared to **PBE**. Depending on the system size, **MTACE** is only 2-4 times slower than **PBE** runs by employing the combination of **MTACE** and CP Groups when a sufficiently large number of processors is used. The best case scenar-

ios for the systems with 32, 64 and 128 water molecules are having **MTACE** runs clocking only 2.7, 3.5 and 4.3 times slower than **PBE**, respectively. Further, **MTACE** is giving a 4-5 fold speed-up compared to **PBE0** when using the highest number of CP Groups we employed. For a 32 water system, the computing time for one MD step is now only 0.86 s for hybrid functional based BOMD with the **MTACE** method when 7680 compute-cores were taken. Figure 5 shows the improved performance of the method with and without the CP Group approach. Similar enhancement in performance is also seen for systems with 64 and 128 water molecules. These results are encouraging as we can generate long trajectories at the level of hybrid functionals within a shorter time by making use of large computing resources. The best computing performances we obtained are 48, 15 and 4 ps of trajectory per day for systems with 32, 64 and 128 water molecules, respectively (see also Figure 7). We would like to emphasize that  $\delta t = 0.48$  fs was taken considering that H atoms were assigned 1 amu mass. By using a deuterium

**Table 5**

Decomposition of total computational time per SCF step for periodic systems containing 32, 64 and 128 water molecules. Various contributions to  $t_{s-ACE}^{SCF}$  and  $t_{s'-ACE}^{SCF}$  are reported.  $t_{SCDM}$  or  $t'_{SCDM}$  is the time for the localization procedure.  $t_{QR}$  is the time for the QR factorization and  $t_{other}$  is the compute time for the rest of the part.  $t_{comput}$  is the compute time for the actual computation of the HF exchange energy. All compute times reported here are in seconds.

$N_{water}$	$N_{CPG}$	$t_{s-ACE}^{SCF}$	$t_{SCDM}$		$t_{comput}$	$t_{s'-ACE}^{SCF}$	$t'_{SCDM}$		$t_{comput}$
			$t_{QR}$	$t_{other}$			$t_{QR}$	$t_{other}$	
32	1	2.14	0.46	0.04	1.65	2.27	0.00	0.03	2.23
	2	2.17	0.93	0.06	1.18	1.67	0.01	0.05	1.62
	4	1.60	0.94	0.06	0.60	0.87	0.01	0.05	0.82
	8	1.39	0.93	0.06	0.40	0.62	0.01	0.05	0.56
	16	1.24	0.94	0.05	0.25	0.39	0.01	0.05	0.33
	32	1.15	0.93	0.05	0.17	0.28	0.01	0.05	0.22
	64	1.12	0.94	0.05	0.13	0.22	0.01	0.05	0.16
64	1	19.61	5.10	0.24	14.27	20.27	0.01	0.20	20.06
	2	12.52	5.00	0.23	7.29	10.46	0.01	0.19	10.25
	4	8.66	4.92	0.21	3.52	5.11	0.02	0.19	4.90
	8	6.90	4.90	0.22	1.78	2.61	0.02	0.19	2.40
	16	6.16	4.89	0.22	1.05	1.54	0.02	0.19	1.33
	32	5.95	4.89	0.21	0.85	1.28	0.03	0.18	1.07
	64	5.72	4.90	0.21	0.61	0.93	0.04	0.18	0.70
128	128	5.62	4.90	0.21	0.51	0.76	0.04	0.18	0.53
	1	183.01	32.57	1.26	149.18	212.59	0.13	1.03	211.43
	2	104.11	32.01	1.24	70.87	102.83	0.13	1.02	101.68
	4	65.23	31.72	1.19	32.32	47.26	0.13	1.01	46.11
	8	49.24	31.67	1.19	16.38	23.61	0.13	1.01	22.46
	16	41.70	31.64	1.18	8.89	12.94	0.14	1.01	11.79
	32	39.44	31.63	1.17	6.65	9.95	0.15	0.99	8.81
256	64	37.41	31.64	1.17	4.60	6.81	0.16	0.99	5.66
	128	36.32	31.65	1.17	3.50	5.20	0.18	0.98	4.03
	256	35.92	31.69	1.17	3.06	4.61	0.26	0.99	3.36

mass for H atoms, a  $\delta t = 1$  fs could be used, resulting in doubling the simulation performance (ps/day).

Our calculations show that the scaling behavior of **s-MTACE** deteriorates beyond a certain number of compute cores. In order to understand this poor scaling behavior, we have looked at the average computing time per SCF step during different modes of force calculations. We label the average computing times per SCF step during the computation of  $\mathbf{F}^{exact}$  and  $\mathbf{F}^{s-ACE}$  as  $t_{exact}^{SCF}$ , and  $t_{s-ACE}^{SCF}$ , respectively. We observe that  $t_{s-ACE}^{SCF}$  scales poorly when CP Groups is large (Table 4). To scrutinize the poor scaling of  $t_{s-ACE}^{SCF}$ , we decomposed the time for various stages of computation (Table 5 and Figure 6). The parallel QR factorization with the ScaLAPACK routines ( $t_{QR}$ ) contributes mostly to the computational overhead for the SCDM localization procedure ( $t_{SCDM}$ ). It is clear that  $t_{QR}$  scales poorly with  $N_{CPG}$ , resulting in an overall poor scaling of  $t_{SCDM}$ . On the other hand, computation of the HF exchange integrals ( $t_{comput}$ ) scales well with  $N_{CPG}$ .

To overcome this and to improve the scalability we adopted the **s'-MTACE** method. The reported results in Table 5 and Figure 6 suggest that the QR factorization with

the ScaLAPACK routine now consumes negligible amount of computing time. As a result, the poor scaling of  $t_{QR}$  has no significant effect on the overall scaling of the method. It has to be noted that the pre-screening procedure used in the **s'-MTACE** method slightly deteriorates the localization properties of the computed SCDMs, resulting in a large number of overlapping pairs during the construction of the ACE operator. Consequently,  $t_{comput}$  turns out to be higher than that of the **s-MTACE** scheme. The overall scaling behavior of MD timings ( $t_{s'-MTACE}$ ) is satisfactory as can be seen in Table 4 and Figure 3.

## 4. Summary

We have presented a detailed benchmarking study on the computational performance of the **MTACE** and **s-MTACE** algorithms with task-groups (CP Group) for performing AIMD simulations with hybrid density functionals and plane waves. In our implementations of the **MTACE** and **s-MTACE** methods using the CP Group environment in the CPMD program, orbital pairs are distributed across the processor groups to achieve a better scaling performance. Through this implementation, we are able to accomplish ex-



## Performance Scaling

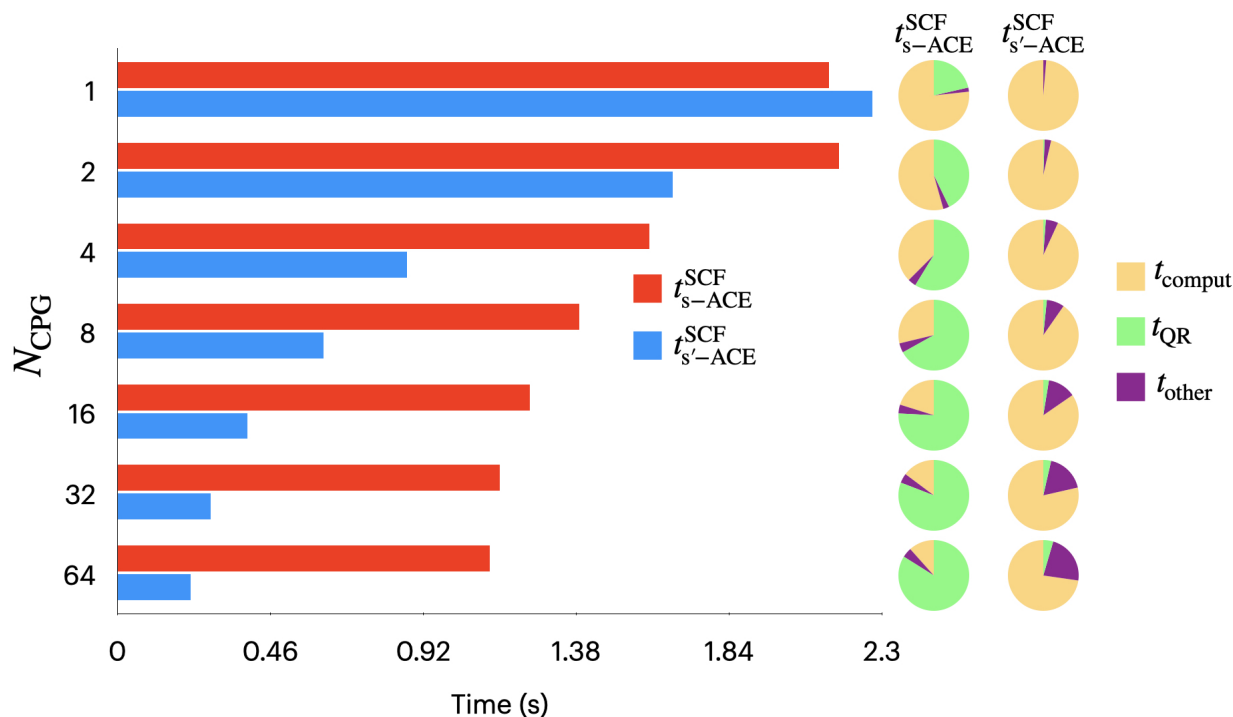


**Figure 6:** Scaling performance of computational time per SCF step for s-MTACE and s'-MTACE with number of CP Group ( $N_{\text{CPG}}$ ) for the periodic 32 water model. Pie charts show the percentage of time spent for different contributions in one SCF step. Here,  $t_{\text{QR}}$  is the computational time for QR factorization,  $t_{\text{other}}$  is the computational time for the rest, and  $t_{\text{comput}}$  is the time for the actual computation of the HF exchange energy.

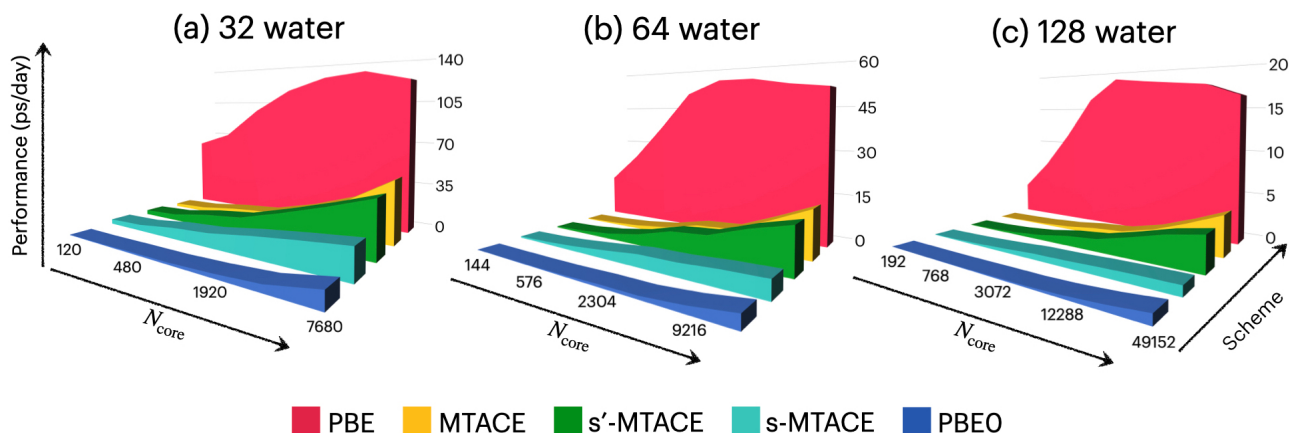


**Figure 7:** Performance measured in units of ps per day for periodic systems containing (a) 32, (b) 64 and (c) 128 water molecules. X axis denotes number of compute cores ( $N_{\text{core}}$ ) and Y axis is indicating different methods described in this article. Z axis is ps of trajectory that can be generated per day using all of these schemes.

cellent scaling behavior beyond  $\sim 100$  compute cores, even for typical system sizes with  $\sim 100$  atoms. Further, excellent speed-up has been also seen while using this implementation. In the best performance achieved for a model system containing 32 water molecules, computational overhead for doing hybrid density functional based AIMD is only 3 times more expensive than with GGA. Our implementation has resulted in boosting the performance of hybrid functional based AIMD of this system by a factor of 121 (see Figure 5). The performance of the s-MTACE method was better than

the MTACE for a small number of CP Groups, however, it deteriorated with increasing number of the CP Groups. This problem was overcome by the implementation of the s'-MTACE method. Our results suggest that either the MTACE or s'-MTACE method in combination with CP Groups is ideal for running hybrid density functional based AIMD simulations on high-performance computers. For system with finite band gap, s'-MTACE should perform better than MTACE.

## Acknowledgement

Financial support from the National Supercomputing Mission (Subgroup Materials and Computational Chemistry) and Science and Engineering Research Board (India) under the MATRICS scheme (Ref. No. MTR/2019/000359) and from the German Research Foundation (DFG) through Research Unit FOR 1878 (funCOS) and Collaborative Research Center SFB 953 (project number 182849149) are gratefully acknowledged. RK thanks the Council of Scientific & Industrial Research (CSIR), India for her Junior Research Fellowship (JRF). Computational resources were provided by SuperMUC-NG (project pn98fa) at Leibniz Supercomputing Centre (LRZ).

## References

- [1] D. Marx and J. Hutter, *Ab Initio Molecular Dynamics: Basic Theory and Advanced Methods* (Cambridge University Press, Cambridge, 2009).
- [2] M. E. Tuckerman, *Statistical Mechanics: Theory and Molecular Simulation* (Oxford University Press, Oxford, 2010).
- [3] A. P. Leach, *Molecular Modelling. Principles and Applications* (Pearson Education Limited, Upper Saddle River, New Jersey, 2001).
- [4] D. Frenkel and B. Smit, *Understanding Molecular Simulation: From Algorithms to Applications* (Academic Press, San Diego, 2002).
- [5] M. E. Tuckerman and G. J. Martyna, *J. Phys. Chem. B* **104**, 159 (2000), URL <https://doi.org/10.1021/jp992433y>.
- [6] A. J. Cohen, P. Mori-Sánchez, and W. Yang, *Science* **321**, 792 (2008), ISSN 0036-8075, URL <http://science.sciencemag.org/content/321/5890/792>.
- [7] P. Mori-Sánchez, A. J. Cohen, and W. Yang, *Phys. Rev. Lett.* **100**, 146401 (2008), URL <https://link.aps.org/doi/10.1103/PhysRevLett.100.146401>.
- [8] W. Koch and M. C. Holthausen, *A Chemist's Guide to Density Functional Theory* (WILEY-VCH, New York, 2001).
- [9] R. M. Martin, *Electronic Structure: Basic Theory and Practical Methods* (Cambridge University Press, Cambridge, 2004).
- [10] A. D. Becke, *J. Chem. Phys.* **98**, 5648 (1993), URL <https://doi.org/10.1063/1.464913>.
- [11] J. P. Perdew, M. Ernzerhof, and K. Burke, *J. Chem. Phys.* **105**, 9982 (1996), URL <https://doi.org/10.1063/1.472933>.
- [12] J. Heyd, G. E. Scuseria, and M. Ernzerhof, *J. Chem. Phys.* **118**, 8207 (2003), URL <https://doi.org/10.1063/1.1564060>.
- [13] C. Adamo and V. Barone, *J. Chem. Phys.* **110**, 6158 (1999), URL <https://doi.org/10.1063/1.478522>.
- [14] C. J. Cramer and D. G. Truhlar, *Phys. Chem. Chem. Phys.* **11**, 10757 (2009), URL <http://dx.doi.org/10.1039/B907148B>.
- [15] B. G. Janesko, T. M. Henderson, and G. E. Scuseria, *Phys. Chem. Chem. Phys.* **11**, 443 (2009), URL <http://dx.doi.org/10.1039/B812838C>.
- [16] Q. Wan, L. Spanu, F. Gygi, and G. Galli, *J. Phys. Chem. Lett.* **5**, 2562 (2014), URL <https://doi.org/10.1021/jz501168p>.
- [17] A. J. Cohen, P. Mori-Sánchez, and W. Yang, *Chem. Rev.* **112**, 289 (2012), URL <https://doi.org/10.1021/cr200107z>.
- [18] H. Xiao, J. Tahir-Kheli, and W. A. Goddard III, *J. Phys. Chem. Lett.* **2**, 212 (2011), URL <https://doi.org/10.1021/jz101565j>.
- [19] Q. Zhao and H. J. Kulik, *J. Phys. Chem. Lett.* **10**, 5090 (2019), URL <https://doi.org/10.1021/acs.jpclett.9b01650>.
- [20] N. Gerrits, E. W. F. Smeets, S. Vuckovic, A. D. Powell, K. Doblhoff-Dier, and G.-J. Kroes, *J. Phys. Chem. Lett.* **11**, 10552 (2020), URL <https://doi.org/10.1021/acs.jpclett.0c02452>.
- [21] B. G. Janesko and G. E. Scuseria, *J. Chem. Phys.* **128**, 244112 (2008), URL <https://doi.org/10.1063/1.2940738>.
- [22] G. F. Mangiatordi, E. Brémond, and C. Adamo, *J. Chem. Theory Comput.* **8**, 3082 (2012).
- [23] T. Todorova, A. P. Seitsonen, J. Hutter, I.-F. W. Kuo, and C. J. Mundy, *J. Phys. Chem. B* **110**, 3685 (2006), URL <http://dx.doi.org/10.1021/jp055127v>.
- [24] C. Zhang, D. Donadio, F. Gygi, and G. Galli, *J. Chem. Theory Comput.* **7**, 1443 (2011), URL <http://dx.doi.org/10.1021/ct2000952>.
- [25] R. A. DiStasio Jr., B. Santra, Z. Li, X. Wu, and R. Car, *J. Chem. Phys.* **141**, 084502 (2014), URL <https://doi.org/10.1063/1.4893377>.
- [26] B. Santra, R. A. DiStasio Jr., F. Martelli, and R. Car, *Mol. Phys.* **113**, 2829 (2015), URL <https://doi.org/10.1080/00268976.2015.1058432>.
- [27] A. Bankura, B. Santra, R. A. DiStasio Jr., C. W. Swartz, M. L. Klein, and X. Wu, *Mol. Phys.* **113**, 2842 (2015), URL <https://doi.org/10.1080/00268976.2015.1059959>.
- [28] F. Ambrosio, G. Miceli, and A. Pasquarello, *J. Phys. Chem. B* **120**, 7456 (2016), URL <https://doi.org/10.1021/acs.jpcc.6b03876>.
- [29] S. Mandal and N. N. Nair, *J. Comput. Chem.* **41**, 1790 (2020), URL <https://onlinelibrary.wiley.com/doi/abs/10.1002/jcc.26222>.
- [30] S. Mandal, V. Thakkur, and N. N. Nair, *J. Chem. Theory Comput.* **17**, 2244 (2021), URL <https://doi.org/10.1021/acs.jctc.1c00009>.
- [31] S. Mandal, J. Debnath, B. Meyer, and N. N. Nair, *J. Chem. Phys.* **149**, 144113 (2018).
- [32] S. Chawla and G. A. Voth, *J. Chem. Phys.* **108**, 4697 (1998), URL <https://doi.org/10.1063/1.476307>.
- [33] X. Wu, A. Selloni, and R. Car, *Phys. Rev. B* **79**, 085102 (2009), URL <https://link.aps.org/doi/10.1103/PhysRevB.79.085102>.
- [34] M. Chen, L. Zheng, B. Santra, H.-Y. Ko, R. A. DiStasio Jr., M. L. Klein, R. Car, and X. Wu, *Nat. Chem.* **10**, 413 (2018), ISSN 1755-4330, URL <GotoISI>://WOS:000428212900008.
- [35] F. Gygi, *Phys. Rev. Lett.* **102**, 166406 (2009), URL <https://link.aps.org/doi/10.1103/PhysRevLett.102.166406>.
- [36] F. Gygi and I. Duchemin, *J. Chem. Theory Comput.* **9**, 582 (2013), URL <http://dx.doi.org/10.1021/ct3007088>.
- [37] W. Dawson and F. Gygi, *J. Chem. Theory Comput.* **11**, 4655 (2015), URL <http://dx.doi.org/10.1021/acs.jctc.5b00826>.
- [38] A. P. Gaiduk, C. Zhang, F. Gygi, and G. Galli, *Chem. Phys. Lett.* **604**, 89 (2014), ISSN 0009-2614, URL <http://www.sciencedirect.com/science/article/pii/S0009261414003170>.
- [39] A. P. Gaiduk, F. Gygi, and G. Galli, *J. Phys. Chem. Lett.* **6**, 2902 (2015), URL <https://doi.org/10.1021/acs.jpclett.5b00901>.
- [40] H.-Y. Ko, J. Jia, B. Santra, X. Wu, R. Car, and R. A. DiStasio Jr., *J. Chem. Theory Comput.* **16**, 3757 (2020), URL <https://doi.org/10.1021/acs.jctc.9b01167>.
- [41] H.-Y. Ko, B. Santra, and R. A. DiStasio Jr., *Enabling large-scale condensed-phase hybrid density functional theory based ab initio molecular dynamics II: Extensions to the isobaric-isenthalpic and isobaric-isothermal ensembles* (2020), arXiv:2011.07209. arXiv.org ePrint archive. <https://arxiv.org/abs/2011.07209> (accessed on December 31, 2020), 2011.07209.
- [42] M. Guidon, F. Schiffmann, J. Hutter, and J. VandeVondele, *J. Chem. Phys.* **128**, 214104 (2008), URL <https://doi.org/10.1063/1.2931945>.
- [43] E. Liberatore, R. Meli, and U. Rothlisberger, *J. Chem. Theory Comput.* **14**, 2834 (2018), URL <https://doi.org/10.1021/acs.jctc.7b01189>.
- [44] S. Fatehi and R. P. Steele, *J. Chem. Theory Comput.* **11**, 884 (2015), URL <https://doi.org/10.1021/ct500904x>.
- [45] S. Mandal and N. N. Nair, *J. Chem. Phys.* **151**, 151102 (2019), URL <https://doi.org/10.1063/1.5125422>.
- [46] M. P. Bircher and U. Rothlisberger, *J. Phys. Chem. Lett.* **9**, 3886 (2018), URL <https://doi.org/10.1021/acs.jpclett.8b01620>.
- [47] M. P. Bircher and U. Rothlisberger, *Comput. Phys. Commun.* **247**, 106943 (2020), ISSN 0010-4655, URL <http://www.sciencedirect.com/science/article/pii/S0010465519302942>.
- [48] V. Bolnykh, J. M. H. Olsen, S. Meloni, M. P. Bircher, E. Ippoliti, P. Carloni, and U. Rothlisberger, *J. Chem. Theory Comput.* **15**, 5601 (2019), URL <https://doi.org/10.1021/acs.jctc.9b00424>.
- [49] J. Vinson, *J. Chem. Phys.* **153**, 204106 (2020), URL <https://doi.org/10.1063/5.0030493>.
- [50] G. F. von Rudorff, R. Jakobsen, K. M. Rosso, and J. Blumberger, *J. Chem. Theory Comput.* **13**, 2178 (2017), URL <https://doi.org/>

- 10.1021/acs.jctc.6b01121.
- [51] L. E. Ratcliff, A. Degomme, J. A. Flores-Livas, S. Goedecker, and L. Genovese, *J. Phys.: Condens. Matter* **30**, 095901 (2018), URL <http://stacks.iop.org/0953-8984/30/i=9/a=095901>.
- [52] V. Weber, C. Bekas, T. Laino, A. Curioni, A. Bertsch, and S. Futral, in *2014 IEEE 28th International Parallel and Distributed Processing Symposium* (Phoenix, AZ, USA, May 19-23, 2014), pp. 735–744, ISSN 1530-2075.
- [53] I. Duchemin and F. Gygi, *Comput. Phys. Commun.* **181**, 855 (2010), ISSN 0010-4655, URL <http://www.sciencedirect.com/science/article/pii/S0010465509004135>.
- [54] N. Varini, D. Ceresoli, L. Martin-Samos, I. Girotto, and C. Cavazzoni, *Comput. Phys. Commun.* **184**, 1827 (2013), ISSN 0010-4655, URL <http://www.sciencedirect.com/science/article/pii/S0010465513001008>.
- [55] T. A. Barnes, T. Kurth, P. Carrier, N. Wichmann, D. Prendergast, P. R. Kent, and J. Deslippe, *Comput. Phys. Commun.* **214**, 52 (2017), ISSN 0010-4655, URL <http://www.sciencedirect.com/science/article/pii/S0010465517300085>.
- [56] L. Lin, *J. Chem. Theory Comput.* **12**, 2242 (2016), URL <https://doi.org/10.1021/acs.jctc.6b00092>.
- [57] W. Hu, L. Lin, A. S. Banerjee, E. Vecharynski, and C. Yang, *J. Chem. Theory Comput.* **13**, 1188 (2017), URL <https://doi.org/10.1021/acs.jctc.6b01184>.
- [58] A. Damle, L. Lin, and L. Ying, *J. Chem. Theory Comput.* **11**, 1463 (2015), URL <http://dx.doi.org/10.1021/ct500985f>.
- [59] I. Carnimeo, S. Baroni, and P. Giannozzi, *Electron. Struct.* **1**, 015009 (2019), URL <https://doi.org/10.1088/2516-1075/aaf7d4>.
- [60] J. Hutter and A. Curioni, *ChemPhysChem* **6**, 1788 (2005), URL <https://chemistry-europe.onlinelibrary.wiley.com/doi/abs/10.1002/cphc.200500059>.
- [61] *CPMD, version 4.3*, Copyright 2000-2019 jointly by IBM Corp. and by Max Planck Institute, Stuttgart. (????), <http://www.cpmd.org> (accessed on December 31, 2020).
- [62] M. Tuckerman, B. J. Berne, and G. J. Martyna, *J. Chem. Phys.* **97**, 1990 (1992), URL <https://doi.org/10.1063/1.463137>.
- [63] P. Giannozzi, O. Andreussi, T. Brumme, O. Bunau, M. B. Nardelli, M. Calandra, R. Car, C. Cavazzoni, D. Ceresoli, M. Cococcioni, et al., *J. Phys.: Condens. Matter* **29**, 465901 (2017), URL <http://stacks.iop.org/0953-8984/29/i=46/a=465901>.
- [64] P. Giannozzi, O. Baseggio, P. Bonfà, D. Brunato, R. Car, I. Carnimeo, C. Cavazzoni, S. de Gironcoli, P. Delugas, F. Ferrari Ruffino, et al., *J. Chem. Phys.* **152**, 154105 (2020), URL <https://doi.org/10.1063/5.0005082>.
- [65] T. Klöffel, G. Mathias, and B. Meyer, *Comput. Phys. Commun.* **260**, 107745 (2021), ISSN 0010-4655, URL <http://www.sciencedirect.com/science/article/pii/S0010465520303684>.
- [66] J. P. Perdew, K. Burke, and M. Ernzerhof, *Phys. Rev. Lett.* **77**, 3865 (1996), URL <https://link.aps.org/doi/10.1103/PhysRevLett.77.3865>.
- [67] N. Troullier and J. L. Martins, *Phys. Rev. B* **43**, 1993 (1991), URL <https://link.aps.org/doi/10.1103/PhysRevB.43.1993>.
- [68] J. Kolafa, *J. Comput. Chem.* **25**, 335 (2004), ISSN 1096-987X, URL <http://dx.doi.org/10.1002/jcc.10385>.